Flow in valve covered orifice nozzles with cylindrical and tapered holes and link to cavitation erosion and engine exhaust emissions

M Gavaises*
City University London, Northampton Square, London, UK

Abstract: Results from a research programme addressing the development, testing, and production of valve covered orifice (VCO) nozzles operating with current production Tier 3 off-highway diesel engines are reviewed. The common rail injectors operate at pressures exceeding 1300 bar and include pilot and main injection events. Although acceptable engine exhaust emissions can be obtained with conventional VCO nozzles, cavitation erosion may lead to mechanical failure of the nozzle. Redesigning the injector in terms of its durability against surface erosion has been obtained through use of a computational fluid dynamics (CFD) flow solver incorporating a two-phase cavitation model and flow visualization in enlarged transparent nozzle replicas. The model has provided evidence of the flow distribution under realistic pressure and needle lift opening scenarios while at the same time it has been calibrated to indicate the locations where the possibility of cavitation erosion may become significant. The experiments performed in enlarged transparent nozzle replicas have provided evidence of the string cavitation structures formed inside the different nozzle designs. Cross-correlation with engine emission tests indicates that string cavitation may be associated with increased engine exhaust emissions. Proposed injector designs with geometric modification easily implemented in the production series have been proved to be erosion-free while at the same time have improved the engine exhaust emissions.

Keywords: valve covered orifice nozzles, cavitation erosion, engine exhaust emissions, CFD flow solver

1 INTRODUCTION

Legislation in Europe and in the rest of the world is set to impose further restrictions on the level of emissions permitted from diesel engines in both the domestic and commercial sectors. The main difficulty posed for the automotive engineering community is how to achieve the new requirements, which involve the simultaneous reduction of NO_x and particulates, while reducing noise and fuel consumption. Computational fluid dynamics (CFD) has become an integral part of the analysis and design of automotive products [**1**–**3**]. Furthermore, it is well known that the performance and exhaust emissions of direct injection (DI) diesel engines are strongly affected by the nozzle flow exit characteristics, which control the atomization process of the injected fuel and the subsequent spray development.

Under most operating conditions cavitation occurs inside the injector nozzle [**4**]; this is generally accepted as one of the most important parameters affecting fuel spray atomization [**5**,**6**]. At the same time, increased injection pressures and multiple injections may result in unsteady cavitation within the fuel system, which might have implications for erosion. According to references [**7**] and [**8**] combination and further optimization of a number of technologies, including the shape and manufacturing of tapered nozzles with smaller hole sizes, will be needed to meet future emission legislation. However, it is known that nozzle cavitation is a transient

phenomenon even under steady state operating conditions, while its effect on the spray structure is still not well understood.

Cavitation is predominantly of the geometric type, although the vortex type (known as 'string cavitation') is also encountered [**9**]. It is also known that the implosion of cavitation bubbles causes, given sufficient time, severe erosion on the material surface of hydrodynamic equipment [**10**, **11**]. Depending on its structure, the material is locally deformed, loosened, and eventually eroded in particles in various ways. The mechanism that is believed to cause this phenomenon is the frequent strain arising from the pressure waves created partly by the microjet and partly by the local shockwaves that are induced by bubble collapse. For this reason, diesel nozzles are susceptible to cavitation erosion and fatigue, given the fact that these phenomena can lead to catastrophic failure of the injectors [**12**]. Moreover, the fact that cavitation can also inflict damage on hydraulic equipment [**13**] makes imperative the assessment and improvement in terms of erosion resistance of materials that could be used for the manufacture of such equipment.

Regarding theoretical works on cavitation erosion, only a limited number exists. In reference [**14**] a Rayleigh model for a single collapsing bubble was developed with assumed toroidal shape including a harmonics analysis in relation to potential erosion caused by such a bubble. In a recent study [**15**] an analytical model for the prediction of cavitation erosion of ductile materials was presented. The basis for the model is a physical analysis of the work-hardening process due to the successive bubble collapses. However, given the complicated flow structures developing inside diesel injectors operating under realistic injection pressures and needle lift traces, including multiple injections, it is practically impossible to make real-time measurements of the acoustic pressures resulting from the collapse of cavitation bubbles and which can be considered responsible for the damage. Qualitative and quantitative information for the cavitating flow parameters can be obtained from computational fluid dynamics models. In this study, cavitation is modelled using the Lagrangian model of references [**16**] and [**17**]. The model has been applied to the simulation of diesel fuel injection systems that have been found to suffer from erosion [**18**]. To represent operating conditions as closely as possible to the actual engine environment, measured injection pressure and needle lift traces have been used, both for pilot and main injection events.

Parallel to the simulation work, evidence of the cavitation structures formed in the particular nozzle geometries investigated is provided from flow visualization studies with large-scale transparent nozzle replicas. As previously reported in reference [**9**], among other published studies, dynamic flow similarity based simultaneously on the Reynolds and cavitation numbers can be applied to provide better understanding of the cavitation formation and development. These data not only provide confidence to the applicability of the computer model to the systems investigated here but also correlate well with the cavitation regimes responsible for specific erosion patterns identified by inspecting damaged nozzles after a long enough running time. Although the available tools cannot predict erosion quantitatively, it has been possible to derive qualitative information on conditions that may indicate higher possibility for damage. This is achieved by comparing instantaneous and time-averaged surface parameters, such as the vapour volume fraction and its standard deviation, as well as the acoustic pressure resulting from the collapse of the cavitation bubbles. Verification for the applicability of the method has been achieved through its application to a nozzle than, although it cavitates, is erosion-free and where the value of these parameters is found to be at much lower levels [**18**].

The present paper is an extension of the work reported recently in reference [**18**] and reviews results obtained from a research programme set up to resolve simultaneously the cavitation erosion problem while satisfying the engine exhaust emission requirements. The technological challenge encountered as part of the development of current production Tier 3 off-highway engines, where significant cavitation erosion has been observed at the entry to and inside the atomizer holes. The erosion severity was deemed unacceptable for continuing long-term production and thus an injector redesign was considered necessary to reduce the erosion to an acceptable level. The effectiveness of a number of redesigns has been durability tested on engines. Out of these, an injector design with a modified needle shape has provided a substantial reduction in the erosion severity and frequency of its occurrence [**18**]. However, emissions and performance testing on the engine has shown that they cause a deterioration in the PM versus NO_x+HC trade-off characteristic.

The deterioration in emissions capability precludes certain ratings from achieving the long-term emissions legislation compliance requirements. The problem statement can be thus set as follows: what

injector design changes are required to give acceptable emissions, without compromising engine performance and with cavitation erosion control? As part of the investigation, both cylindrical as well as tapered nozzle holes have been employed. Tapered nozzle holes are known to suppress cavitation and thus suffer less or completely eliminate cavitation erosion. The findings from the present study have demonstrated that the dynamic or string cavitation formation and development may be responsible for increased engine exhaust emissions. Formation of such structures is enhanced with a specific combination of the needle valve shape and the tapered nozzle holes.

The next section of the paper describes briefly the computation model, the flow test rig as well as the nozzle geometries and operating conditions tested. Then, the results obtained are presented, followed by the most important conclusions.

2 RESEARCH TOOLS

As mentioned, both computational fluid dynamics models predicting cavitation as well as visualization studies in transparent enlarged nozzles have been employed for understanding the flow development in the specific nozzles under investigation. A brief description of the modelled physical processes as well as a description of the visualization rig is given.

2.1 Computational model

The developed and validated Eulerian–Lagrangian cavitation model is presented in detail in references [**16**] and [**17**]; thus, mathematical details are not repeated here. Also, the details of the specific models and flow processes considered can be found in reference [**18**] for the same nozzle designs. Here, only a brief summary of the computational model is given below.

The in-house GFS RANS flow solver, as modified in reference [**16**], has been used to simulate the flow inside the nozzles tested. This model is capable of simulating the geometric-induced hole cavitation but not string cavitation; thus, model predictions can be used only to complement the experimental results, in order to assist in the interpretation of the obtained images. For the liquid phase the volume and ensemble-averaged continuity and Navier–Stokes equations are solved. As a result of the dynamic interaction of the cavitation bubbles with the surrounding pressure field the available volume for the liquid phase can change significantly. The effect of the additional vapour is taken into account by including the liquid phase volume fraction α_l (referred to as the 'liquid fraction') in the conservation equations. Moreover, due to the slip velocity between the cavitation bubbles and the flowing liquid, there is additional interaction which is taken into account with the inclusion of the appropriate source terms in the conservation equations

$$\frac{\partial}{\partial t}(\alpha_L \rho_L) = \tilde{N}(\alpha_L \rho_L \boldsymbol{u}_L) = 0 \tag{1}$$

$$\frac{\partial(\alpha_L \rho_L \boldsymbol{u}_L)}{\partial t} + \tilde{N}\left(\alpha_L \rho_L \boldsymbol{u}_L \ddot{A} \boldsymbol{u}_L\right) = -\tilde{N}\rho + \alpha_L \tilde{N}\left\{(\mu_L + \mu_t)\left[\tilde{N}\ddot{A}\boldsymbol{u}_L + \left(\tilde{N}\ddot{A}\boldsymbol{u}_L\right)^T\right]\right\} + \boldsymbol{s}_{\text{momentum}} \tag{2}$$

where μ_t is the eddy viscosity, calculated as $\mu_t = C_\mu \rho_L \left(k_L^2/\varepsilon_L\right)$.

In equation (2) with the term $\boldsymbol{s}_{\text{momentum}}$ the effect of the cavitation bubbles' relative motion upon the liquid phase is taken into account. Although a model that can address the combined effect of turbulence and cavitation on the flow has as yet not appeared, nozzle flows are highly turbulent and the standard two-equation k–ε has been employed for the consideration of turbulence effects. Additional effects of the bubbles' relative movement on the liquid phase turbulent kinetic energy and dissipation are also included. It has to be noted that as part of the numerous numerical tests that have been performed during the development of the model, a number of other turbulence models have been tested, apart from the standard k–ε, namely the re-normalisation group theory (RNG) of reference [**19**] and the a non-equilibrium version of reference [**20**] as applied in the simulation of cavitating flows [**21**].

In single-phase calculations of nozzle flows with injection and backpressures corresponding to cavitation numbers high enough for cavitation to be present, the location of its inception is identified from the numerical cells where the pressure falls below vapour pressure. The volume of all the Eulerian grid cells where pressure is below that of vapour is referred to as 'tension volume' and provides a quantitative indication of how much liquid is stretched due to the flow. Cavitation initiates and then further develops the existence of small spherical bubble nuclei assumed to pre-exist within the liquid, following a preassigned size and number distribution according to reference [**22**].

The model is based on the Eulerian–Lagrangian approach, while the liquid phase is modelled as the continuous phase and the cavitation bubbles as the dispersed one. Many of the fundamental physical processes assumed to take place in cavitating flows are incorporated into the model. These include bubble formation through nucleation, momentum exchange between the bubbly and the carrier liquid phase, bubble growth and collapse due to non-linear dynamics according to the early study of reference [**23**], bubble turbulent dispersion as proposed in reference [**24**], and bubble turbulent/hydrodynamic break-up, based on the experimental observations of reference [**25**]. The effect of bubble coalescence and bubble-to-bubble interaction on the momentum exchange and during bubble growth/collapse is also considered. More details and a thorough validation of the model can be found in references [**16**] and [**17**].

The second-order Crank–Nicolson discretization scheme has been employed for modelling the time derivatives of the solved equations. The time step used for the simulation of the nozzle volume flow has been varied between 10^{-4} and 10^{-5} s, which is short enough to capture the transient development of the vortices formed inside the nozzle. However, a much shorter time step of 0.5×10^{-7} s has been used for simulating the cavitation structures formed inside the injection hole. It has to be noted that an adaptive time step with values down to 10^{-12} s is used in the integration of the Rayleigh–Plesset equation proposed in reference [**26**], for simulating the growth and collapse of the cavitation bubbles. Regarding spatial discretization, the second-order scheme of reference [**27**] has been used in addition to the first-order hybrid scheme. Fully unstructured numerical grids consisting of tetrahedral and hexahedral elements have been used.

The cavitation model has an inherent transient characteristic and thus transient simulations are performed even for fixed needle lift and steady pressure boundary conditions. This is due to the nature of cavitation formation and collapse processes, which deviate from thermodynamic equilibrium conditions. Cavitation is initiated when the predicted pressure falls below the vapour pressure of the working fluid. When the second vapour (bubbly) phase is introduced into the system of the solved equations, the pressure recovers from the values below the vapour pressure, which obviously are a prerequisite for the incipience of cavitation, towards the threshold limit above which nucleation of new bubbles stops. The number of bubbles forming depends on the liquid available locally for nucleation. This result in an inherently transient pattern to the formation of bubbles since when more vapour is present, the local pressure recovers towards the nucleation threshold value, which in turn reduces the amount of cavitation formed.

This adds to the time-dependent and explosive growth/collapse process which the bubbles undergo once they have been formed. Time-averaging over the pilot and/or main injection duration period can lead to estimation of a locally mean vapour volume distribution but also to its standard deviation. That can allow identification of designs associated with more or less stable cavitation patterns. For the purposes of the present investigation, where surface erosion is to be related with the development of the cavitation, predicted values on the surface on the nozzle are recorded.

In addition, the so-called 'acoustic pressure', calculated as

$$P_{\text{acoustic}} = \frac{\rho}{4\pi\ell}\left(\frac{\mathrm{d}^2V}{\mathrm{d}t^2}\right)$$

in reference [**11**] has been further estimated on the wall surface. In this equation, V is the bubble volume, ρ the liquid density, t stands for time, and l the distance of the bubble from the wall. The value of the acoustic pressure to be presented in the following sections has been calculated as the sum of the contribution from all bubbles during their tracking time step. An average value has been calculated over the pilot and main injection pulses. The values of this integral quantity are normalized relative to those obtained for the standard VCO nozzle with cylindrical holes; these will be referred to as relative acoustic pressure. It will be shown later that all these three parameters can indicate in relative terms conditions that are more likely to result in cavitation erosion.

2.2 Flow visualization

Transparent nozzles were manufactured from an acrylic material. The flow rig utilized is that of references [**9**] and [**28**]; all relevant details can be found there. The working fluid was water at 25 °C. The flowrate of water was controlled by a valve in the pipe downstream of the feed pump and measured by an orifice plate flowmeter. The flowrate from each of the injection holes was also measured simultaneously with the incoming flowrate. Both the injection pressure and the pressure downstream of

the injection holes were adjusted by restricting the inflow and outflow of the injector respectively. In order to reach subatmospheric backpressures and therefore higher cavitation (CN) and Reynolds (*Re*) numbers, a suction pump was installed in addition to the main feed pump. The Reynolds number has been defined on the basis of the mean flowrate and average hole diameter while the cavitation number is defined here as $CN = (P_{INJ} - P_{BACK})/(P_{BACK} - P_V)$.

Since it is important to gain knowledge about the dynamics of the cavitation inception and formation processes for various flow conditions, a high-speed digital video system was set up. For the particular cases investigated here, usually 6000 to 16 000 fps were sufficient to capture the temporal development of cavitation using a shuttering time of 30 μs. In total up to 4000 images were collected for a particular case. A strong halogen floodlight together with some halogen spotlights were necessary to provide enough light for the intensified charge coupled device (CCD) video chip in combination with the high frame rates.

3 TEST CASES

All injector designs investigated are fundamentally the same. They are a single-fluid common rail design that uses a three-way, solenoid-actuated control valve. The pressure in the nozzle group is at (or close to in the case of injections preceded by a close-coupled injection) injector drain pressure between injections. The nozzle itself is a VCO design (Fig. 1(a)). The nominal hole diameter may range according to the desired flowrate of the nozzle; the value used for the present investigation is 0.175 mm.

For this nozzle, two sites of surface erosion have been identified and are shown in the scanning electron microscope (SEM) images of the atomizer tip, in Figs 1(b) and (c) respectively. The first one is found at the top part of the hole close to its entry. This image shows an extreme example produced by accelerated testing at elevated rail pressure. The second erosion site has been observed at the 3 and 9 o'clock positions of the hole entrance, as shown in Fig. 1(c). This time, the surface damage is extended upstream of the injection hole inside the sac volume. The other nozzle geometries to be reported here are shown in Fig. 2. Starting from the original VCO nozzle of Fig. 2(a), the modified needle design has a groove in the needle. Results for this design relative to the original one have been reported in reference [**18**].

Although the flow through this nozzle has resulted in significantly reduced cavitation formation and collapse during the opening and closing stages of the needle, increased engine exhaust emissions have made application of this nozzle more difficult. The HC emissions with the VCO-grooved nozzle are generally higher.

The conclusion that might be drawn from this is that the HC emissions performance of injectors improves with time. It is clear that the poor HC performance of the grooved nozzle compared with the standard VCO nozzle has a substantial detrimental effect on the NO_x+HC versus PM trade-off. This is true in respect of its effect on the nominal difference in the trade-off curves and also the injector set-to-injector set variability. Tests were carried out using stochastic process modelling (SPM). For each nozzle variant, the best NO_x+HC versus particulate trade-off curve was obtained within the bounds of maximum rail pressure, timing, and cylinder pressure limits, and the end of injection limits. However, the same pilot quantity and dwell were used in each case. The rail pressure range across the datum points was 76–110 MPa. The SPMs

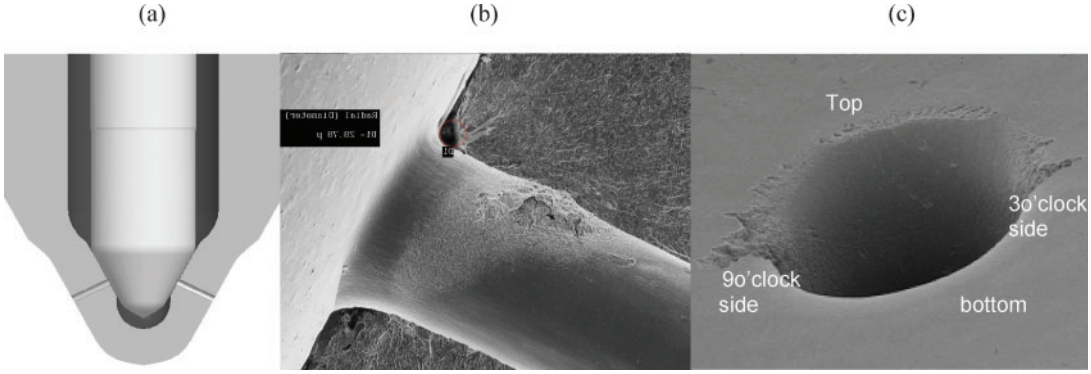

Fig. 1 (a) Schematic of the VCO nozzle investigated, (b) picture of erosion damage at the top part of the injection hole, and (c) erosion damage at the two sides of the injection hole (from reference [**18**])

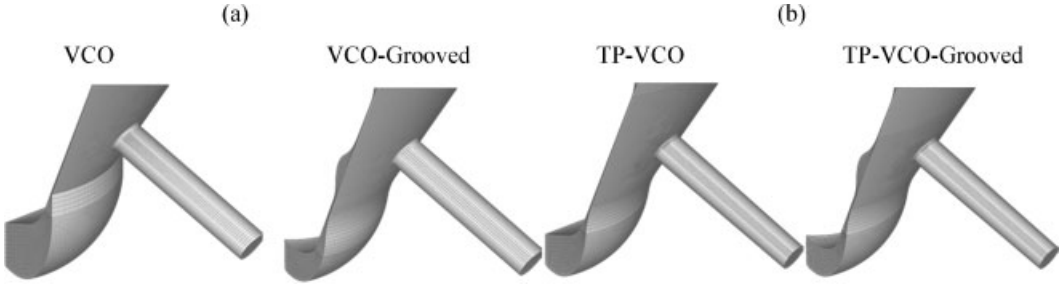

Fig. 2 Numerical grid of the 60° sector of the VCO nozzle designs investigated: (a) cylindrical hole nozzle and (b) tapered hole nozzle. For each nozzle, two different needle shapes have been tested, one with a flat needle as shown and one incorporating a recovery groove

for each injector type were carried out on the same engine.

The new results to be reported here relative to those of the original designs refer to the two tapered holes of Fig. 2(b). These nozzles are identical to those of Fig. 2(a), but the converging tapered holes greatly modify the pressure distribution within the nozzle, and as a result the formation of cavitation and erosion damage. Despite that, engine exhaust emissions have been improved only with the nozzle without the grooved needle. The results to be reported here provide observations of the flow characteristics in these nozzles, which are fundamentally different due to the formation of string cavitation.

As mentioned, enlarged transparent nozzle replicas have been manufactured for all nozzle designs investigated; a sample photograph and a bottom-view picture of the large-scale model layout can be seen in Figs 3(a) and 3(b), respectively, while Fig. 3(c) shows the geometric characteristics of the tapered nozzle hole. The operating conditions tested for the two large-scale transparent nozzles are summarized in Table 1. As can be seen, cavitation numbers between 0.5 and 10 have been tested, which are similar to those of the real-size injector operating under engine operating conditions. Imaging was performed for various combinations of the listed parameters and for different needle lifts. The values to be reported here correspond to equivalents of 20, 100, and 250 μm of the actual nozzle.

The measured and calculated discharge coefficients of all four large-scale nozzles are shown in Fig. 4. The recovery groove has only a very small effect on the nozzle discharge coefficient. However, the tapered hole nozzles have a much higher discharge coefficient, as expected. In order to keep the fuel injection quantity and injection duration the same between the cylindrical and the tapered holes, the exit diameter of these nozzles was significantly reduced compared with the cylindrical ones, down to 162 μm. On the same plot, predictions from the CFD model are also included; these results are indicated with two horizontal bars. The upper bar corresponds with predictions obtained with the single-phase flow solver and exhibits values a little higher than those predicted using the cavitation model of reference [**29**]. As mentioned above, this model accounts for the

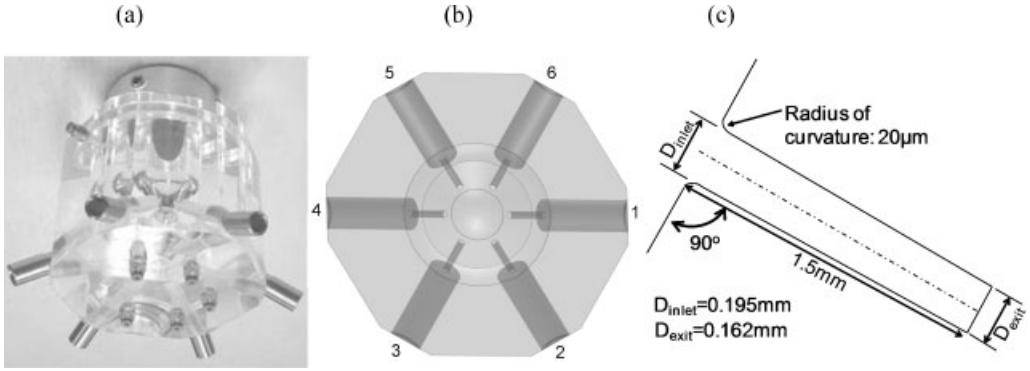

Fig. 3 (a) Photograph of the ×15 enlarged fully transparent nozzle replica used for visualization of cavitation inside the injection holes, (b) bottom view of the transparent nozzle indicating the injection holes numbering and expansion tubes, and (c) tapered nozzle hole geometric characteristics

Table 1 Operating conditions for the large-scale nozzles

	Pressure (bar)							
	Inlet		Back		Cavitation number		Reynolds number	
Needle lift (μm)	Minimum	Maximum	Minimum	Maximum	Minimum	Maximum	Minimum	Maximum
20	2.6	7.1	0.6	1.2	2	10.4	10 600	36 000
100	2.8	5.9	0.6	1.3	1.2	8	26 800	48 700
250	4.8	4.8	0.55	0.55	8.5	8.5	60 000	60 000

geometric-induced cavitation forming at the hole inlet due to the sharp pressure drop in this area. The model indicates that cavitation may be responsible for up to 8 per cent reduction in the nozzle discharge coefficient at low needle lifts while its relative importance increases with the increased amount of cavitation. This is the case of the cylindrical hole nozzle at the highest needle lift setting. As mentioned, there is no cavitation for the same lift when tapered holes are employed, so in this case only one horizontal bar is depicted. Overall, model predictions are close to the experimental values and thus model predictions can be considered reliable for providing more detailed information about the flow distribution inside the nozzle; more thorough validation of the CFD model used can be found in reference [**17**] and more recently in reference [**30**].

Regarding the nozzle flow simulation performed for the real-size nozzles, the operating conditions used for the simulation are presented in Fig. 5. This graph shows the injection pressure and needle lift diagram used. A fixed 50 bar pressure value has been used at the exit of both nozzles. The model requires as inputs some initial values for the submodels used; as mentioned above, a detailed description can be found in reference [**18**]. Only one-sixth of the injector has been simulated, as shown previously in Fig. 2. The numerical grid consists of approximately 600 000 numerical cells. For simulating the transient motion of the needle valve, two grids have been made at 30 and 150 μm. For needle lifts greater than 150 μm the second grid was stretched while for needle lifts lower that 150 μm, stretching of the first grid is performed; remapping of the solution between the two grids is required at 150 μm while the minimum needle lift considered was 5 μm. To simulate operating conditions lower than this lift, the flow rate values for these conditions have been used. Finally, the working liquid was diesel fuel with a density of 835 kg/m^3 and dynamic viscosity of 2.5×10^{-3} kg/m s.

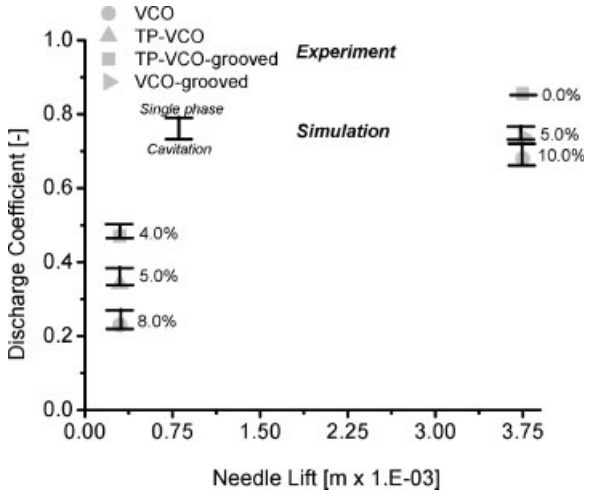

Fig. 4 Measured and calculated nozzle discharge coefficient as a function of needle lift for the different enlarged nozzle model designs investigated

4 RESULTS AND DISCUSSION

In this section sample results from the various parametric studies performed are reviewed. The first important finding regarding the internal nozzle flow in the cylindrical and tapered nozzle holes is summarized in Fig. 6. This figure shows representative images of the observed cavitation in all four nozzle replicas considered, for all three needle lift values investigated. Clear differences can be observed not only between the cylindrical and the

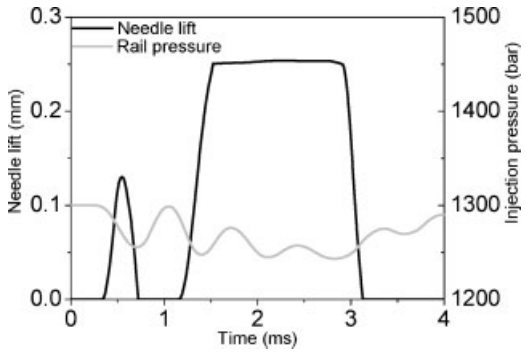

Fig. 5 Injection pressure, backpressure, and needle lift used for the pilot and main injection events for all test cases simulated (from reference [**18**])

tapered holes but also between the two different needles. The standard VCO nozzle exhibits formation of a cavitation cloud at the hole inlet, which seems to collapse within the injection hole. Increasing needle lift results in fully developed cavitation, which extends up to the hole exit. The VCO nozzle with the grooved needle shows that at low needle lift the formed cavitation is a combination of the geometric cavitation formed at the hole inlet, but also string cavitation, which extends up to the hole exit. This is very clear in the images collected in the tapered nozzle. There, string cavitation dominates the flow at low and intermediate lifts while cavitation disappears completely at high needle lifts. Cavitation strings are much more evident in the grooved designs rather than in the standard needle. It is thus clear that the groove enhances the formation of string cavitation.

Evidence of the flow distribution in the real-size injector including the motion of the needle valve and the pulsating fuel rail pressure is provided by the computational model. Figures 7 and 8 show the predicted mean cavitation volume fraction and its standard deviation respectively on the surface of the injection hole. Two averages have been performed, one for the pilot and one for the main injection event. The results indicate that more cavitation is calculated with the standard needle design. The standard deviation plots indicate a much more fluctuating cavitation structure with the standard needle and, in particular, for the pilot injection event. Results for the relative acoustic pressure, shown in Fig. 9, indicate much higher levels of this parameter for the standard nozzle. The peak level of this parameter coincides with the erosion site inside the injection hole, as revealed with the SEM image of

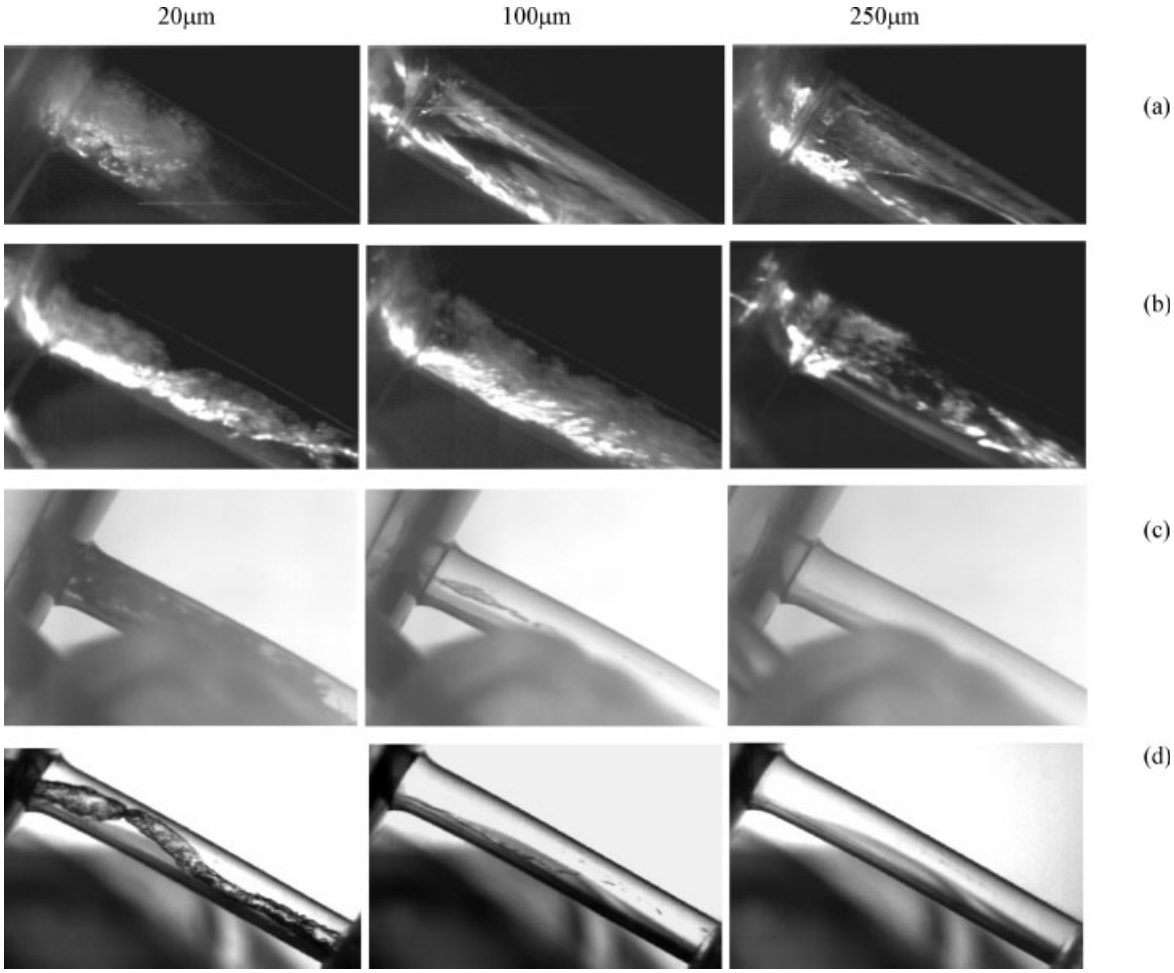

Fig. 6 Sample representative images of cavitation structures formed in the injection hole of the various nozzle designs investigated at three different needle lifts equivalent to 20, 100, and 250 μm of the real-size nozzle: (a) VCO nozzle, (b) VCO nozzle with a needle groove, (c) tapered VCO nozzle, and (d) tapered VCO nozzle with a needle groove

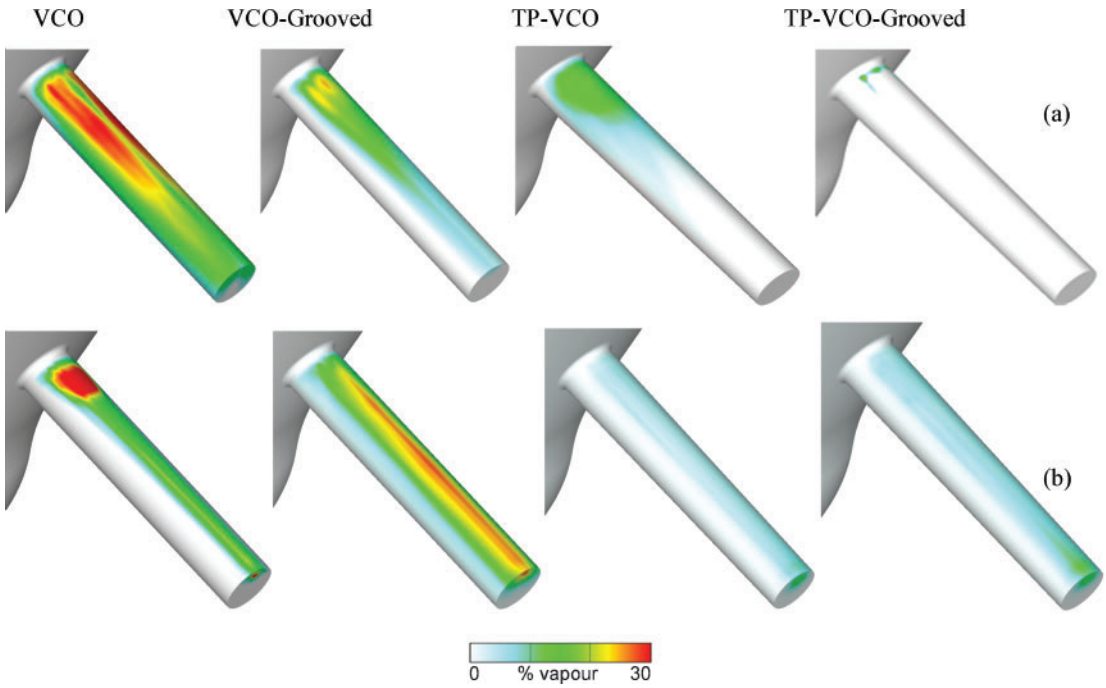

Fig. 7 Predicted time-averaged mean cavitation vapour volume fraction distribution on the nozzle hole wall surface for the different designs investigated for (a) pilot injection and (b) main injection

Fig. 1(b). All other three designs that have been found to be free from cavitation erosion after a sufficient running time also indicate much lower acoustic pressure levels. It is thus clear that the groove allows for the flow to turn more easily inside the injection holes, which has been found to

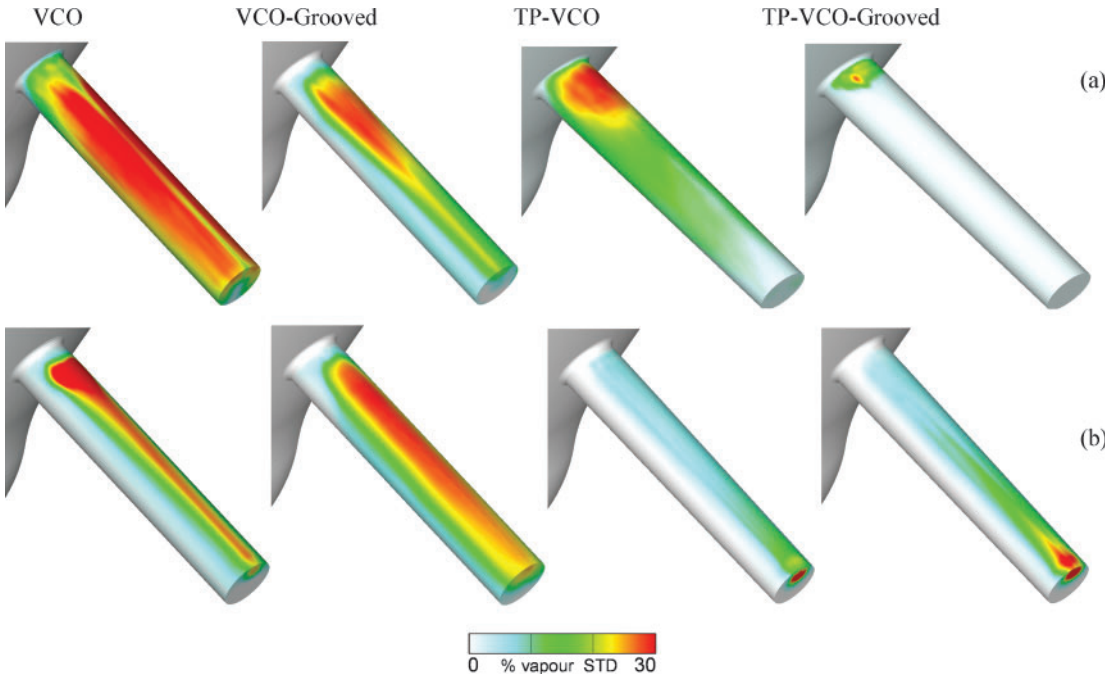

Fig. 8 Predicted time-averaged standard deviation of mean cavitation vapour volume fraction distribution on the nozzle hole wall surface for the different designs investigated for (a) pilot injection and (b) main injection

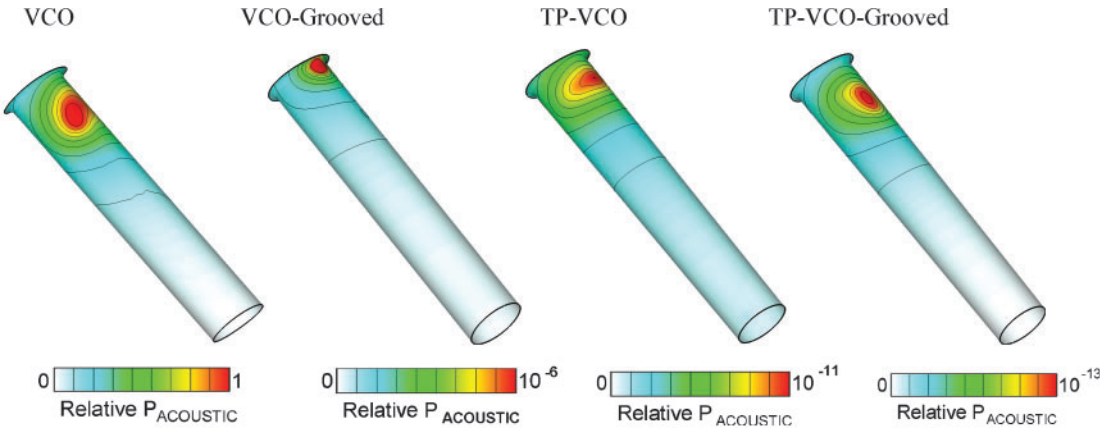

Fig. 9 Predicted time-averaged relative acoustic pressure on the nozzle hole wall surface for the different designs investigated for pilot injection

eliminate cavitation erosion, while tapered holes further suppress formation of cavitation and eliminate erosion.

This can be further interpreted from Fig. 10, which shows the temporal evolution of the percentage of the hole exit cross-section occupied by cavitation. Predictions are shown only for the pilot injection event. A sharp increase in the amount of cavitation produced from the opening and closing of the needle valve can be observed for the standard nozzle geometry at the early stages of the opening and closing of the needle valve. The grooved-needle nozzle reduces this overshoot of cavitation vapour to levels similar to those realized with the tapered hole nozzle using the standard needle. A combination of both tapered-hole and grooved-needle nozzles almost eliminates the formation of cavitation, even at the stages of needle movement.

As already mentioned, unfortunately there is no model that can predict at present the formation of string cavitation, which seems to be enhanced by the

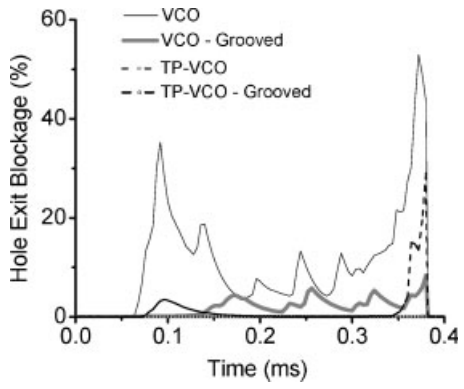

Fig. 10 Predicted temporal evolution of hole exit blockage for the four designs investigated (pilot injection, from reference [**33**])

presence of the groove and even more of tapered holes. Thus, information about these flow structures can be obtained only experimentally. It seems, though, that they do not contribute significantly to surface erosion. Apart from the fact that the grooved nozzle (which exhibits cavitation strings) satisfied the durability tests, the flow images obtained in the enlarged nozzle models indicate that a cavitation string develops at the central part of the injection hole, and thus do not collapse near the wall surface.

In relation to these observations, it is of importance to comment on the engine exhaust emissions. These are summarized in Fig. 11, which shows the soot–NO_x trade-off curve for all four designs. It is clear that the injectors with an increased appearance of string cavitation seem to give higher emissions than those with the 'conventional' and repeatable geometric hole cavitation.

This is likely to be due to the addition of the recovery groove. The recovery groove not only increases the parasitic volume below the check seat but also substantially reduces the length of the clearance path between the sac and the holes when the needle valve is seated. The reduced length of the clearance path would make it easier for the volume of the fuel in the sac to be drawn into the cylinder after the needle has been reseated at the end of injection. The variability is also higher with this nozzle. In addition, HC emissions increase with reducing load. This may be due to the lower cylinder pressures and temperatures at lower loads, causing the atomization characteristic towards the end of injection to deteriorate and allowing carryover of unburnt fuel into the exhaust. The rate of change in HC with load is greater with the grooved nozzle. This may be due to the lower pressure at the entry to the atomizer holes expected with the grooved design.

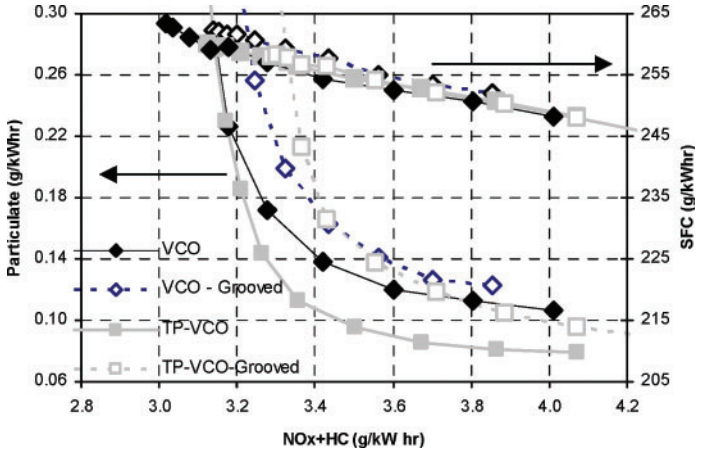

Fig. 11 Measured engine exhaust soot–NO_x trade-off for the different nozzle designs investigated

These hydraulic, atomization, and combustion characteristics are consistent with the relevant literature.

Although there is no direct evidence from spray characterization studies for the particular injectors investigated here, results reported in references [**31**] and [**32**] have clearly shown that the presence of string cavitation greatly modifies the spray angle in a rather chaotic manner. That, in turn, is expected to affect the spray development further downstream and at the end combustion and engine exhaust emissions.

5 CONCLUSIONS

This paper has reviewed results from a research programme undertaken for the development, testing, and production of VCO nozzles operating with current production Tier 3 off-highway diesel engines. The focus of the investigation was on the effect of injector design on (a) the internal nozzle flow and (b) the engine performance and exhaust emissions. In particular, the common rail injector incorporating the standard VCO nozzle has shown cavitation erosion problems at specific operation modes, which have included pilot and main injection events. Simulation of the flow with an in-house CFD cavitation model has indicated that the observed cavitation damage correlates well with areas of bubble collapse; the relative magnitude of a surface parameter, referred to as 'acoustic pressure', has been demonstrated to be indicative of the cavitation erosion sites.

As part of redesigning the injector in terms of its durability, different needle shapes have been tested as well as nozzles with tapered holes. Specific needle shapes incorporating a groove facing the injection holes have been proved to modify the flow distribution during the opening phase of the needle valve and eliminate cavitation erosion. Nozzles with tapered holes also suppress formation of geometric cavitation and have also been proved erosion-free.

However, experiments performed in enlarged transparent nozzle replicas have provided evidence of string cavitation structures formed inside the different nozzle designs. The nozzles with the grooved needle have been found to enhance formation of string cavitation, in an unsteady and non-repeatable mode. The formation of cavitation strings was maximized at lower lifts of the grooved needle in the tapered hole nozzle. Interestingly enough, the grooved nozzle designs dominated by string cavitation have been found to result in increased engine exhaust emissions, while nozzles with tapered converging holes have been found to satisfy both durability to surface erosion and engine exhaust emissions.

ACKNOWLEDGEMENTS

The authors would like to thank Mr A. Mr Andriotis, Mr D. Papoulias, and Mr N. Mitroglou from City University London for their contribution to the research programme.

REFERENCES

1 **Senecal, P. K., Montgomery, D. T.,** and **Reitz, R. D.** A methodology for engine design using multidimensional modelling and genetic algorithms with validation through experiments. *Int. J. Engine Res.*, 2000, **1**, 229–248.

2 **Canakci, M.** and **Reitz, R. D.** Experimental optimization of a DI–HCCI–gasoline engine using split

injections with fully automated microgenetic algorithms. *Int. J. Engine Res.*, 2003, **4**(1), 47–60.

3 **Liu, Y.** and **Reitz, R. D.** Optimizing HSDI diesel combustion and emissions using multiple injection strategies. SAE paper 2005-01-0212, 2005.

4 **Giannadakis, E.** and **Gavaises, M.** Modelling of cavitation in large scale diesel injector. In 19th Annual Meeting of the Institute for Liquid Atomization and Spray Systems (Europe), Nottingham, 2004.

5 **Soteriou, C., Andrews, R.,** and **Smith, M.** Direct injection diesel sprays and the effect of cavitation and hydraulic flip on atomization. In Society of Automotive Engineers, Technical Paper Series, 1995.

6 **Tamaki, N.**, *et al.* Effects of cavitation and internal flow on atomization of a liquid jet. *Atomization and Sprays*, 1998, **8**, 179–197.

7 **Soteriou, C.**, *et al.* The flow characteristics of high efficiency diesel nozzles with enhanced geometry holes. In THIESEL 2006 Conference on *Thermo- and fluid dynamic processes in diesel engines*, Valencia, Spain, 2006.

8 **Desantes, J.**, *et al.* Experimental characterization of internal nozzle flow and diesel spray behavior. Part I: non-evaporative conditions. *Atomization and Sprays*, 2005, **15**(5), 517–544.

9 **Roth, H., Gavaises, M.,** and **Arcoumanis, C.** Cavitation initiation, its development and link with flow turbulence in diesel injector nozzles. *SAE Trans. J. Engines,* 2002-01-0214, 2002, **111**(3), 561–580.

10 **Knapp, R. T., Daily, J. W.,** and **Hammitt, F. G.** *Cavitation*, 1970 (McGraw-Hill, New York, London).

11 **Brennen, C. E.** *Cavitation and bubble dynamics*, 1995 (Oxford University Press, Oxford, New York).

12 **Asi, O.** Failure of a diesel engine injector nozzle by cavitation damage. *Engng Failure Analysis*, 2006, **13**(7), 1126–1133.

13 **Escaler, X., Dupont, P.,** and **Avellan, F.** Experimental investigation on forces due to vortex cavitation collapse for different materials. *Wear*, 1999, **235**, 65–74.

14 **Prikhodko, V. M.**, *et al.* Modelling of cavitational erosion in the area of surfaces of smooth contact. *Ultrasonics Sonochem.*, 2001, **8**(1), 59–67.

15 **Berchiche, N., Franc, J. P.,** and **Michel, J. M.** A cavitation erosion model for ductile materials. *Trans. ASME, J. Fluids Engng*, 2002, **124**(3), 601–606.

16 **Giannadakis, E.** *Modelling of cavitation in automotive fuel injector nozzles*, PhD Thesis, Imperial College, University of London, 2005.

17 **Giannadakis, E.**, *et al.* Evaluation of the predictive capability of diesel nozzle cavitation models. SAE paper 2007-01-0245, 2007.

18 **Gavaises, M.**, *et al.* Link between cavitation development and erosion damage in diesel fuel injector nozzles. SAE paper 2007-01-0246, 2007.

19 **Yakhot, V.**, *et al.* Development of turbulence models for shear flows by a double expansion technique. *Physics of Fluids A*, 1992, **4**(7), 1510–1520.

20 **Shyy, W.**, *et al. Computational techniques for complex transport phenomena*, 1997 (Cambridge University Press, New York).

21 **Vaidyanathan, R.**, *et al.* Sensitivity evaluation of a transport-based turbulent cavitation model. *Trans. ASME, J. Fluids Engng*, 2003, **125**(3), 447–458.

22 **Meyer, R. S., Billet, M. L.,** and **Holl, J. W.** Freestream nuclei and traveling-bubble cavitation. *Trans. ASME, J. Fluids Engng*, 1992, **114**(4), 672–679.

23 **Prosperetti, A.** and **Plesset, M. S.** Vapour-bubble growth in a superheated liquid. *J. Fluid Mechanics*, 1978, **85**(2), 349–368.

24 **Farrell, K. J.** Eulerian/Lagrangian analysis for the prediction of cavitation inception. *Trans. ASME, J. Fluids Engng*, 2003, **125**(1), 46–52.

25 **Martínez-Bazán, C., Montañés, J. L.,** and **Lasheras, J. C.** On the breakup of an air bubble injected into a fully developed turbulent flow. Part 2: size PDF of the resulting daughter bubbles. *J. Fluid Mechanics*, 1999, **401**, 183–207.

26 **Plesset, M. S.** and **Prosperetti, A.** Bubble dynamics and cavitation. *Annual Rev. Fluid Mechanics*, 1977, **9**, 145–185.

27 **Papadakis, G.** and **Bergeles, G.** A locally modified 2nd-order upwind scheme for convection terms discretization. *Int. J. Numer. Meth. for Heat and Fluid Flow*, 1995, **5**(1), 49–62.

28 **Roth, H.** *Experimental and computational investigation of cavitation in diesel injector nozzles*. PhD Thesis, Imperial College, University of London, 2004.

29 **Giannadakis, E., Gavaises, M.,** and **Arcoumanis, C.** Modelling cavitation in diesel injector nozzle holes. *J. Fluid Mechanics*, 2008 (accepted).

30 **Giannadakis, E.**, *et al.* Simulation of cavitation in outwards opening pintle injectors. *Proc. IMechE, Part D: Automobile Engineering*, 2008 (accepted).

31 **Gavaises, M.** and **Andriotis, A.** Cavitation inside multi-hole injectors for large diesel engines and its effect on the near-nozzle spray structure. *SAE Trans. J. Engines,* 2006-01-1114, 2006, **115**(3), 634–647.

32 **Andriotis, A.** and **Gavaises, M.** Influence of vortex flow and cavitation on near-nozzle diesel spray dispersion angle. *Atomization and Sprays*, 2008 (accepted).

33 **Gavaises, M.**, *et al.* Comparison of cavitation formation and development in diesel VCO nozzles with cylindrical and converging tapered holes. In THIESEL 2008 Conference on *Thermo- and fluid-dynamic processes in diesel engines*, Valencia, Spain, 9–12 September 2008.

APPENDIX

Notation

l	length/distance
P_{BACK}	downstream pressure
P_{INJ}	injection pressure
P_V	vapour pressure
Re	Reynolds number
t	time
V	volume
μ_L	dynamic viscosity
ρ_L	liquid density

Abbreviations

CCD	charged coupled device
CFD	computational fluid dynamics
CN	cavitation number
DI	direct injection
PM	particulate matter
SEM	scanning electron microscope
SPM	statistical parametric mapping
TP	tapered
VCO	valve covered orifice